





29 2016) through debris flows, debris floods, debris slides, etc. The likelihood of post-fire debris flows  
30 increases in proportion with burn severity (Jordan, 2016). Post-fire debris flows are caused mainly by  
31 the runoff-triggered entrainment of hillslope material (Cannon et al., 2001; Santi et al., 2008; Kean et  
32 al., 2011, Parise and Cannon, 2012) and infiltration-triggered meter-scale shallow landslides (Wondzell  
33 and King, 2003; Cannon and Gartner, 2005; Parise and Cannon, 2012). Statistics show that the majority  
34 of post-fire debris flows are triggered by surface water runoff (Gartner, 2005; Parise and Cannon, 2012;  
35 DeGraff et al., 2015), especially in the first 1~2 summers after a wildfire, when large quantities of ash  
36 from burned vegetation and unaggregated fine-grained dry ravel are susceptible to overland runoff or  
37 debris flows. As time passes, the underground roots decay, and more infiltration-triggered meter-scale  
38 shallow landslides emerge and transform into debris flows (Jordan, 2016; DeGraff et al., 2015).

39 Surface water runoff can be generated when the rainfall intensity is greater than the infiltration  
40 rate. Wildfire can quickly destroy the vegetation in mountainous areas, making it possible for rainwater  
41 to directly reach the earth rather than being intercepted by the canopy (Robichaud, 2000; Wondzell and  
42 King, 2003; Larsen et al., 2009; Stoof et al., 2012). The sealing of surface soil pores by ash remnants  
43 and other unaggregated fine soil particles can reduce the infiltration capacity of the soil (Larsen et al.,  
44 2009; Woods and Balfour, 2010). In addition, soil water repellence increases after a fire so that the soil  
45 resists wetting for a time and its soil hydraulic ability declines (Doerr and Thomas, 2000; MacDonald  
46 and Huffman, 2004; Doerr et al., 2006; Nyman et al., 2010). The hydraulic conductivity related to soil  
47 sealing, soil water repellency and other hydrological properties (MacDonald and Huffman, 2004;  
48 Moody et al., 2016). Moody et al. (2016) suggest that soil hydraulic conductivity is unchanged and  
49 remains equal to the values for soil unaffected by fire for low burn severity and exponentially decreases  
50 with burn severity when it is high. In short, a change of the surface soil properties caused by wildfire  
51 can significantly decrease the soil hydraulic conductivity and induce greater surface water runoff for a  
52 given amount of rainfall (Robichaud et al., 2000; Onda et al., 2008; Moody and Ebel, 2012; Moody and  
53 Ebel, 2014). In addition, the rainfall threshold for debris flows can greatly decline after a wildfire  
54 (Conedera et al., 2003; Cannon et al., 2008; Moody and Ebel, 2012; Staley et al., 2013).

55 The existing research on post-fire debris flows focuses more on western America (Robichaud et al.,  
56 2000; Cannon et al., 2008; Larsen et al., 2009; Kean et al., 2011; Moody et al., 2016), followed by  
57 southeastern Australia (Lane et al., 2006; Nyman et al., 2010; Smith et al., 2010); British Columbia,  
58 Canada (VanDine et al., 2005; Jordan, 2016); and Switzerland (Conedera et al., 2003). In western China,



59 certain debris flows affected by wildfire have been reported in Yangfan (Yunan Province) in the 1970s,  
60 Jiarongka (Sichuan Province) in 2015 and Reneyong (Sichuan Province) in 2014 and 2015; however, no  
61 detailed research has previously been conducted. This manuscript aims to: 1) document the post-fire  
62 debris flows in western China; 2) explore the effects of the inherent climatic, geologic and geomorphic  
63 characteristics on post-fire debris flows; and 3) determine the reasons for the variations in rainfall  
64 threshold among debris flows.

## 65 **2. Study area**

### 66 **2.1 Natural setting**

67 The Reneyong Valley, located in Xiangcheng County in the central Hengduan Mountains of  
68 western China, covers an area of 24.28 km<sup>2</sup> with an outlet to the Dingqu River (which flows into the  
69 Jinsha River, upstream of the Yangtze River) at 29°08'N, 99°33'E (Fig. 1). This catchment has a nearly  
70 equilateral triangular shape and is surrounded by high mountains reaching 4222 m a.s.l. at the  
71 northernmost location and 2855 m a.s.l. at the westernmost location on a fork of the Dingqu River.  
72 There are 9 branches (No. 1~No.9) in this watershed (Fig. 1), and the width of the channels varies  
73 between 2 and 30 m. In general, the branches have V-shaped channels and the main channel is  
74 U-shaped. The geographic information for the three branches where debris flows occur is listed in  
75 Table 1. Branches No. 1, No. 2 and No. 3 are in the southern part of the catchment and have an  
76 elongated shape and a southeast-northwest orientation. Branches No. 1 and No. 2 have a similar  
77 channel gradient, but branch No. 3 is much gentler. The change in gradient along the stream is similar,  
78 with the steepest gradient in the central part and a relatively gentle gradient in the upper and lower  
79 portions.

80 The continental monsoon plateau climate prevails in the study area, with rainfall concentrated  
81 from June to September and plentiful sunshine. According to the statistics of rainfall data from the  
82 Xiangcheng meteorological station (approximately 33 km to the southeast), the mean annual rainfall is  
83 472.62 mm and the mean annual evaporation capacity of 2362 mm is 5.28 times the mean annual  
84 rainfall, indicating that the study area is quite arid. Tall trees, shrubs and herbs cover the entire  
85 watershed, and the majority of the trees are *Pinus densata*.

86 Faults tend to have a north-south orientation, and no single fault extends through the  
87 watershed (Fig. 2). As in the Three Parallel Rivers area, the Neotectonic movement is strong with the



88 uplift of the Tibetan plateau; however, historically, earthquakes in Xiangcheng was reported to be lower  
89 than Ms. 6.0, and the strongest recorded earthquake (Ms. 5.3) occurred on 5 June 1974 in Dongjun  
90 village, 27 km northeast of this catchment. The bed lithology is soft rock and is divided into 4 units (Fig.  
91 2) nearly parallel to the fault: black slate and sandstone of the Triassic system upstream, sandy slate and  
92 some limestone of the Triassic system in the middle stream, black slate and some limestone of the  
93 Triassic system on both sides downstream and alluvial deposits of the Quaternary system on the  
94 channel bed and in the accumulation fan downstream.

## 95 **2.2 Debris flow cases**

96 Ancient debris flow deposits exist in the accumulation fan, indicating historical debris flows.  
97 Interviews with local citizens indicated that no debris flows occurred in the 100 years before 2014,  
98 while at least 4 debris flows have occurred since the wildfire in June 2014 (Table 2).

99 The town of Zhengdou is on the accumulation fan of the Renyong Valley. On 8 June 2014, the  
100 local administrators were holding a seminar on reconstruction after the wildfire and were warned of  
101 debris flows by a patrolman (Jiuli) who was responsible for geological hazards after he had found no  
102 water flows in the channel. This first debris flow is identified as DF1 in this paper. After that debris  
103 flow, the Sichuan Institute of Geological Engineering Investigation was appointed to conduct a field  
104 survey. On 30 June, another debris flow occurred that is identified as DF2. On the night of 10 July 2014,  
105 when we were staying at the local elementary school, we heard the noise of a debris flow collision and  
106 then witnessed the debris flows in the downstream (this event is identified as DF3). On 24 August 2015,  
107 a storm was predicted by the weather report, and the local geologic hazards administrator issued a  
108 warning. Before the debris flows reached the downstream area, the patrolman (Jiuli) again found no  
109 water flows in the channel and warned the local people to escape. This event is identified as DF4.  
110 Fortunately, the 4 debris flows were reported before they reached the village, and although the debris  
111 flows destroyed houses (Fig. 3), roads (Fig. 4) and farmland, leading to an economic loss of 18 million  
112 Yuan, no people were killed.

113 In fact, as stated by a local citizen, in 2014, there were other debris flows rushing out from branch  
114 No. 1, carrying dozens or hundreds of cubic meters of sediment downstream and cutting off the  
115 Xiangcheng-Derong road. As the debris flows did not hit residential areas or destroy other facilities, the  
116 exact time of the debris flows remains unclear. In general, debris flows after the wildfire in Renyong



117 Valley is of high frequency.

### 118 **3. Methods**

#### 119 **3.1 Meteorological data**

120 In western China, most rain gauges are located in the valleys, where there are more residents and  
121 the basic facilities are better, while few exist in the upper areas where debris flows begin. The study site  
122 is in the central Hengduan Mountains, and the nearest three rain gauges, at Zhengdou, Adu and Reda  
123 near the study area, are applied(Fig. 2, Table 3). The first rain gauge, Zhengdou, is on the deposition  
124 fan of the Renyong Valley; the second, Reda, is in another valley on the other side of the southeastern  
125 crest; and the third, Adu, is in the same valley as Reda on the other side of the northeastern crest. The  
126 three rain gauges form a triangle around the study area, monitoring rainfall sources from several sides.  
127 Other information about the three rain gauges is listed in Table 3.

128 As rainfall arriving at the initiation area can be transformed in different ways, rainfall data from  
129 the nearer rain gauge could be more important for determining the average rainfall process. Indeed, the  
130 reciprocal-distance-squared method can be used to deduce the average rainfall process in the initiation  
131 area as follows(Chow et al., 1988; Chen et al., 2012):

$$132 \quad P = \sum_{i=1}^3 \omega_i P_i \quad (1)$$

133 where  $P_i$  is the rainfall record from the rain gauges;  $i=1, 2, \text{ or } 3$  represents the Zhengdou, Reda and  
134 Adu rain gauges, respectively; and  $\omega_i$  is the weighing factor corresponding to  $P_i$ . The weighting

135 factor can be expressed by  $\omega_i = d_i^{-2} / \sum_{i=1}^3 d_i^{-2}$ , where  $d_i$  is the distance from rain gauge  $i$  to the  
136 debris flow initiation area.

#### 137 **3.2 Field survey**

138 After the debris flows, we conducted a field survey to evaluate the impact of the wildfire and  
139 investigated the initiation process and the magnitude of the debris flows to propose debris flow  
140 alleviation strategies. After DF1, we conducted the first field survey and personally witnessed DF2  
141 moving downstream when we were living in the local elementary school. After DF4, we conducted a  
142 second field survey to investigate the debris flow initiation process and examine the impact of debris



143 flows on the check dams to evaluate whether additional work was required to prevent future debris  
144 flows.

145 (1) Detecting the scope of the wildfire

146 We interviewed the local citizens and were informed that the fire was accidentally set by workers  
147 who were building an iron tower for an electrical transmission line at 18:00 on 1 June 2014. After the  
148 fire, fire fighters, armed police and local citizens gathered to fight the fire and it was extinguished at  
149 10:00 on 5 June.

150 After the wildfire, the forest administrators measured the scope of the wildfire. They walked along  
151 its boundary and marked the scope on a contour map (with a scale of 1:100000). According to this map,  
152 an area of 5.4 km<sup>2</sup> in the catchment was affected by the wildfire (Fig. 1), accounting for 22.2% of the  
153 entire watershed. In detail, branches No. 1, No. 2 and No. 3 were within the scope. The majority of the  
154 trees are *Pinus densata*, under which are shrubs and herbs, a good place for yaks and sheep to graze  
155 (Fig. 5).

156 (2) Sediment investigation

157 Our field survey was conducted along the channel, and a laser range finder was applied to gather  
158 measurements. We measured the bank failure and the high erosive deposits along the two sides of the  
159 channel, the bank-failure induced soil slide, and the scope and amount of spoil along the  
160 Xiangcheng-Derong road. We marked these on a contour map and recorded them in a notebook,  
161 respectively. We dug six troughs, 1.5m in length, 0.5 m in width and 0.3~0.6 m in depth (Fig. 6), on the  
162 slope where the wildfire burned to detect the depth of the ashes and the variety and extent of roots  
163 destroyed by the wildfire. We also collected soils from the troughs to measure the particle size  
164 distribution and the natural water content. In addition, a borehole was used to measure the depth of the  
165 debris flow deposits and the loose gravel deposits underneath.

166 (3) Measurement of debris flow deposits

167 The volume of debris flows can be used to evaluate the magnitude, which can be found by  
168 measuring the sporadic deposit division. For each deposit division, we used a laser range finder to  
169 measure the scope and average depth to calculate its volume. The precision of the volume was more  
170 dependent on the measurement of the average depth, which can reach 100 m<sup>3</sup>, thus the volume of each  
171 division larger than 50m<sup>3</sup> would be recorded as 100 m<sup>3</sup>, otherwise, it would be not included.

172 The majority of DF4 is deposited behind two newly built check dams and only a few portions



173 reached downstream by passing through cracks on the check dams. We measured and marked the  
174 boundaries of the deposits on the contour map that was completed during the first field survey before  
175 the check dams were built. We measured the height of the check dams above the deposits and obtained  
176 the depth buried by the deposits, which is the greatest depth of the deposit. We divided the largest  
177 deposit depth into several parts and calculated the volume as follows:

$$178 \quad V = \sum_{i=1}^n h_i A_i \quad (2)$$

179 where  $V$  is the volume of the deposits;  $h_i$  is the height of each part of the deposits;  $A_i$  is the area of  
180 the horizontal area;  $i=1, 2, \dots$ , and  $n$  represents the parts that were divided. Normally, we set  $h_i$   
181 =1m, which means that the deposits from the toe of the dam to the end of the deposit after the dam  
182 were divided into  $n$  parts and that each part had a height of 1m.  $A_i$  is the area circled by the axis of the  
183 dam and the corresponding contour line and can be obtained using a 1:500 contour map.

184 In the deposit zone, we measured particle size and lithology. We placed a ruler of 50 m on the  
185 surface of the deposits randomly. We measured particle size and recorded the lithology of the stones at  
186 a 1-m interval along the ruler (Fig. 7). For particles larger than 60 mm, the diameter and lithology were  
187 recorded, otherwise, only the lithology was recorded. Deposits smaller than 60 mm were collected to  
188 complete particle size distribution tests in the laboratory.

## 189 **4. Analysis and results**

### 190 **4.1 Recorded rainfall process**

191 Before the debris flows daily rainfall data were collected from Zhengdou, Reda and Adu, and the  
192 reciprocal-distance-squared method was applied to obtain the average rainfall (Table 3). Table 2 shows  
193 that in 2014, there was only occasional drizzle in the preceding days and the 3-day accumulated rainfall  
194 was only a few millimeters except in the case of DF3, when it was 14.84 mm. In 2015, it sprinkled for  
195 several days, and the 3-day accumulated rainfall before DF4 reached nearly 40 mm (daily rainfall data  
196 for the day before DF4 is missing because of instrument error, and rainfall data from the Xiangcheng  
197 meteorological station, 33 km to the southeast, were used). In the year that the wildfire occurred, the  
198 3-day accumulated rainfall for the 3 debris flows varied greatly, which suggests that post-fire debris  
199 flows were not correlated with the antecedent rainfall; however, the antecedent rainfall significantly



200 increased in the second summer.

201 Hourly rainfall data before and after the debris flows were collected from Zhengdou, Reda and  
202 Adu, which were applied to determine the average rainfall process by the reciprocal-distance-squared  
203 method. The rainfall processes before and after the four debris flows are depicted in Fig. 8, which  
204 shows there was short-term low-intensity rainfall before the three debris flows in 2014. The rain gauge  
205 worked well, as local administrators discussing reconstruction after the wildfire recalled that only  
206 occasional drizzle had occurred prior to DF1. When we were living in the local elementary school we  
207 witnessed only sprinkles when DF3 occurred. However, it seems impossible for a rainfall intensity of  
208 1mm/h or less to generate sufficient surface runoff and the subsequent debris flows. Instead, local  
209 convective rainfall in the mountains could be the trigger which cannot be recorded by the nearby rain  
210 gauges.

211 On 24 August 2015, the storm began at approximately 19:00, and the average rainfall intensity  
212 reached 26.39 mm/h. In the outlet of the main channel, the rainfall intensity reached 38.5 mm/h and  
213 then declined to less than 5 mm/h. DF4 arrived in the downstream area at approximately 19:43, and if  
214 we deduct the time needed for it to move from the initiation area to the outlet, we find that the debris  
215 flows were likely initiated shortly after the rainfall began.

#### 216 **4.2 Debris flow initiation process**

217 According to the location of the debris flow deposits and the residual scar left by debris flow  
218 erosion, all the debris flows originated in the fire-affected area, with DF1, DF2 and DF3 deriving from  
219 branch No. 3 and DF4 from branches No. 1, No. 2 and No. 3 and some smaller neighboring catchments  
220 on 24 August 2015. However, as some catchments' drainage is too small to depict accurately in Fig. 1,  
221 this paper considers only branches No. 1, No. 2 and No. 3.

##### 222 (1) Debris flows in 2014

223 In 2014, the debris flows were triggered in the upstream area of branch No. 3. Upstream, trunks  
224 were surrounded by charcoal and ashes, and only a few trunks toppled over. Shrubs, herbs and litter  
225 were consumed by the wildfire, and the slope surface was covered by ashes, but the underground root  
226 system survived and the affected soil was concentrated in only a few centimeters. Unaggregated dry  
227 ravel is widely distributed, and dry ravel remnants mixed with ashes were found to have flowed along  
228 the slope, indicating that the entrainment of the surface runoff should be the origin of the debris flows.



229 The channel is only 0.5~0.8 m wide and 0.4~0.6 m deep on a steep slope with exposed stones and no  
230 debris flow deposits (Fig. 9). Items above the channel fell parallel to the channel, suggesting that the  
231 debris flows submerged the entire channel and that the discharge was still smaller than 1 m<sup>3</sup>/s. Erosion  
232 caused by the debris flows is limited by the small discharge, and the transported soil particles were  
233 limited in the smaller debris flows. In the middle stream and downstream areas of branch No. 3, the  
234 channel gradient decreases, while the slope of both sides increases to 35~45°, forming a narrow  
235 V-shaped gully. The moving debris flows entrained the bed sediment and scored the base of the banks,  
236 leading to bank failure on both sides. The intensive scars of landslides with no vegetation can be found  
237 on both sides along the channel. These shallow landslides were meter-scale, with a volume ranging  
238 from tens of cubic meters to thousands of cubic meters. At the beginning, where the channel is quite  
239 narrow, it can be blocked by landslide deposits of a small magnitude; as more sediment is deposited in  
240 the channel, the broadened channel can be partly blocked by a small landslide and entirely blocked by a  
241 large one (Fig. 10). In addition, the burned trunks can favor channel blocking. Channel blocking  
242 alleviates the debris flow process, and the outburst debris flows have a significantly larger discharge  
243 (Cui et al., 2013; Zhu, 2013).

#### 244 (2) Debris flows in 2015

245 The debris flow initiated in branch No. 2 (Fig. 11) is similar to that initiated in branch No. 3, while  
246 that initiated in branch No. 1 (Fig. 12) is slightly different. Shrubs, herbs and the lower parts of the  
247 trees were partly consumed by the wildfire. In the second summer after the wildfire, the trees were  
248 again covered by green crowns. Branch No. 1 can be divided into three parts according to the channel  
249 gradient, with the steepest gradient (32°) in the middle part, where the debris flow was initiated, and a  
250 gentle gradient in the source area. Two smaller gullies converge at the debris flow initiation zone,  
251 forming a platform between them. During the storm, the surface water runoff in the source area  
252 entrained sediment and formed a debris flood. Following the debris flow initiation zone, which is quite  
253 steep, the debris flood from the two gullies had a higher erosion ability; it scored both sides of the  
254 platform and triggered bank failure, followed by the retrogressive meter-scale landslide failure of the  
255 platform. The debris flood mixed with the detached bank slope and formed debris flows; meanwhile,  
256 the 9.2 mm of accumulative rainfall over the previous three days endowed the surface layer with  
257 relatively higher water content, and the retrogressive landslide failure caused it to slide and liquefy into  
258 debris flows. In the lower stream, a debris flow moving over wet sediment can greatly increase



259 sediment entrainment and significantly amplify the magnitude of the flow (Iverson et al., 2011; McCoy  
260 et al., 2012).

### 261 **4.3 Debris flow deposits**

262 The majority of DF1 deposited in the wide section of the channel downstream of the fork with  
263 branch No. 3. Some of it jumped the channel banks and destroyed houses, and the remaining rushed  
264 into the Dingqu River though it did not block the river (Fig. 13a). DF2 traced the previous path, leaving  
265 a slight depth of debris covering the DF1 deposits and striking our borehole instrument (Fig. 13b). The  
266 volume of DF2 is much smaller than that of DF1. DF3 continually traced these deposits and left  
267 considerable deposits in the wide section. DF3 also jumped the river banks and buried some parts of the  
268 road in the residential area and the remaining partially blocked the Dingqu River (Fig. 13c). As two  
269 check dams were completed, the deposits of DF4 are much different. The majority of DF4 was  
270 intercepted by the two check dams except a portion in the mainstream. Debris reached the top of check  
271 dam No. 1 (with a height of 4 m) and only the upper 6 m of check dam No. 2 was above the deposits  
272 (Fig. 13d), leaving the lower 12 m buried by the deposits.

273 Based on field measurements and indoor calculations, we determined the volume of the four  
274 debris flows (Table 2). There are large differences among the volumes of the debris flows, of which, the  
275 volume of DF4 is the largest, reaching 154,500m<sup>3</sup>, followed by DF1 at 86,200m<sup>3</sup>, DF3 at 3,2300 m<sup>3</sup> and  
276 DF2 at 5,100m<sup>3</sup>. Although the volumes of DF2 and DF3 are smaller than that of DF1, they still arrived  
277 downstream and were dangerous, as DF1 had paved a path, and the friction of the stream had decreased  
278 significantly. Statistics show the deposits are angular, and the majority of them are sandy slate  
279 (90.48%), followed by slate (7.14%) and limestone (2.38%), which suggests that the debris flows  
280 originated from branches Nos. 1~3, where sandy slate dominates, and this suggestion is consistent with  
281 our field survey.

## 282 **5. Discussion**

283 Debris flows do not occur in all fire-affected watersheds; instead, the response to rainfall could be  
284 debris flows (in a proportion of 40%) (Cannon, 2001; Nyman et al., 2010; Kean et al, 2011), flash  
285 floods (Cannon, 2001; Kean et al. 2011) or no response (Cannon, 2001; Smith et al. 2010). The debris  
286 flows in the Reneyong Valley are unusual because the debris flows are of high frequency; in addition,  
287 although three debris flows occurred in branch No. 3 in 2014, branches No. 1 and No. 2 had no



288 response to rainfall even though they had steeper gradients and debris flows are more likely to occur in  
289 the first year following wildfire.

290 These facts lead us to believe that the likelihood of debris flows is correlated with the impact of  
291 wildfire but also with the geology, drainage area, channel gradient, and regional climate, which are not  
292 affected by wildfire. In the later discussion, we attempt to discuss these factors to resolve the doubt we  
293 have encountered regarding the post-fire debris flows in the Reneyong Valley.

### 294 **5.1 Rainfall threshold**

295 The 4 post-wildfire debris flows in the Reneyong Valley were generated by surface water runoff.  
296 The rainfall intensity recorded by the downstream rain gauge was 1 mm/h or less and the duration was  
297 quite short, which is in line with the memory of the local citizen in the downstream area who witnessed  
298 the flow, suggesting the rain gauge was working well; however, it seems impossible for a low-intensity  
299 short-duration rainfall to generate surface water runoff, let alone entrain sediment and trigger debris  
300 flows. In the Hengduan Mountains, isolated convective rainfall is common and has been found to be an  
301 important trigger of debris flows in this area (Tang et al., 2011; Ni et al., 2014); in addition, rainfall  
302 intensity has also been found to increase with elevation in the Jinsha Basin (Tan et al., 1994). Here, we  
303 speculate that the three post-wildfire debris flows in 2014 were triggered by isolated convective rainfall  
304 and that the rain gauges down slope can definitely record the triggering rainfall.

305 Observations of debris flows in the Jiangjia Valley show that higher intensity rain can generate  
306 debris flows of larger magnitude, and an exponential increasing model was built (Zhuang et al., 2009)  
307 that might model the process of rainfall amplifying the activity of debris, resulting in more soil slides  
308 and of greater magnitude (Dai and Lee., 2001; Guo et al., 2013). In addition, sediment wetted or  
309 saturated by rainfall is more susceptible to entrainment by debris flows (Iverson, 2011; McCoy et al.,  
310 2012). Similar research can be found in post-wildfire research, just as rainfall totals have been applied  
311 in the magnitude prediction model, other factors, including drainage area and burned areas of high and  
312 moderate severity, have been incorporated (Gartner et al., 2008; Cannon et al., 2010).

313 In a given catchment, we attempted to use the volume of the debris flows to deduce the possible  
314 triggering rainfall as follows: the volume of DF4 is much larger, suggesting the highest triggering  
315 rainfall, followed by DF1, DF3 and DF2, respectively. In a word, low rainfall in 2014 did trigger three  
316 debris flows in branch No. 3, while none occurred in branches No. 1 and No. 2. Greater rainfall in 2015



317 generated debris flows in the three branches, which indicates that the rainfall threshold for post-wildfire  
318 debris flows in the Reneyong Valley was quite low during the first summer after wildfire and that it  
319 increased as time passed. In addition, debris flows in branches No. 1 and No. 2 had a higher rainfall  
320 threshold compared to that of branch No. 3.

## 321 **5.2 Regional climate**

322 Soil water repellency could be of high significance in reducing soil hydraulic conductivity and  
323 amplifying surface water runoff immediately after a wildfire (MacDonald and Huffman, 2004; Doerr et  
324 al., 2006; Moody et al., 2013). It may also inhibit the soil rewetting process (Doerr et al., 2000), which  
325 may require days to weeks and will be quite small or nonexistent in the second summer after a fire  
326 (MacDonald and Huffman, 2004; Larsen et al., 2009). According to our trough test, soil in the burned  
327 area was covered by a centimeter of ashes and the surface layer affected by wildfire was concentrated  
328 in only a few millimeters (Fig. 6), and the soil water repellency of the surface layer should have been  
329 limited, which might have played a key role in triggering DF1 and might have had no effect on DF4.

330 The surface soil could have low water content as a result of the long-duration arid climate, so that  
331 the surface layer could also have low hydraulic conductivity (Moody and Ebel, 2012; Sheridan et al,  
332 2016). This low conductivity may be responsible for the quite low rainfall threshold for the later debris  
333 flows, as rainfall infiltration into the soil is limited and surface runoff can easily occur. Indeed, if a  
334 hyper-dry condition is reached, no rain can infiltrate into the soil (Moody and Ebel, 2012). The effect of  
335 a long-duration arid climate on soil water content could be meter-scale, while the depth of rainfall  
336 infiltration is limited to the surface and the time for the soil to recover aridity could be only days.  
337 Aridity should be a key theme because the drought ravel in steep arid catchments has been identified as  
338 an important source of runoff-triggered debris flows (Kean et al., 2011, 2013; Staley et al., 2014; Noske  
339 et al., 2016).

340 It is highly difficult for vegetation to recover in newly generated landslide scars in an arid climate,  
341 and the uncovered loose sediment can be much more easily entrained by debris flows without the  
342 binding effect of roots (Ziemer, 1981; Gyssels et al., 2005). In general, the increase in soil water  
343 repellency and decline in hydraulic conductivity induced by wildfire should be transient and the effect  
344 of an arid climate on erosion could be perennial, which has been verified in the non-fire-affected area  
345 (Carretier et al., 2013).



### 346 **5.3 Geology and soil properties**

347 Sandy slate from the Triassic system dominated the three branches, accompanied by small  
348 amounts of limestone. Sandy slate is soft and susceptible to the weathering process, resulting in a deep  
349 mantle of soil covering the bedrock with a high fine-particle content and more boulders of limestone.  
350 Based on the field survey of the successive landslide scars along the branches, the sediment is fine  
351 grained, arid and loose, characteristics that make it vulnerable to debris flow entrainment. As the  
352 weathered eluvium is abundant, the channel is charged with sediment, resulting in a high frequency of  
353 debris flows (Bovis and Jakob, 1999; Jakob et al., 2005). In the branches, the underlying bedrock can  
354 hardly be found, and bedrock in some sections of the main channel is uncovered, suggesting that the  
355 downward erosion of debris flows is an important process in the steep branches and that the successive  
356 bank failures are generated by debris flow bulking (Hung et al., 2005; Gabet and Bookter, 2008; Zhu,  
357 2013). These landslides can partly or wholly block the channel, and debris flows can be greatly  
358 amplified after an outburst (Cui et al., 2013; Zhu, 2013).

### 359 **5.4 Channel gradient and drainage area**

360 The three catchments share a similar channel gradient, with the largest gradient in the central part  
361 and smaller gradients in the upper and lower parts (Table 1). This configuration tends to produce a  
362 greater surface runoff for a given rainfall process and to exert higher erosion ability in the middle area  
363 with the largest gradient to produce debris flows of greater magnitude (Coe et al., 2008; McCoy et al.,  
364 2012), as entrainment in steep terrain can increase rapidly with slope owing to both shearing stress and  
365 transport capacity (Foster and Meyer, 1972; Stock and Dietrich, 2003; Hung et al, 2005; Moody et al,  
366 2013; Kean et al, 2013).

367 Drainage area, the scope of the area that rainfall can flow into, is a more dominant factor for the  
368 magnitude of surface runoff. Of the three sub-catchments, branch No. 3 has the largest drainage area,  
369 followed by branches No. 2 and No. 1, each of which has a drainage area smaller than 1 km<sup>2</sup>. In 2014,  
370 the debris flows originated solely in branch No. 3; however, in 2015, debris flows occurred in branches  
371 No. 1~3 and some smaller sub-catchments where the rainfall intensity reached 38.5 mm/h. Here, we  
372 hypothesize that the terrain is similar: a larger area tends to have greater surface water runoff, and the  
373 likelihood of debris flow occurrence could be higher; thus, greater rainfall is required to trigger  
374 post-fire debris flows in a relatively smaller area.



375 This principle should not be applied in all fire-affected areas, as the statistics developed in earlier  
376 studies (Gartner, 2005; Cannon et al., 2010) suggest that post-fire debris flows can occur where the  
377 drainage area is smaller than 25 km<sup>2</sup> and even where it is smaller than 5 km<sup>2</sup>. The reasons may be that  
378 the terrain of a smaller catchment is apt to be steep and the surface water runoff can have higher  
379 erosion ability (Hung et al, 2005; Moody et al, 2013), increasing the susceptibility to debris flow  
380 occurrence; as the drainage area increases, the catchments tend to have wider channels and gentler  
381 gradients (Stock and Dietrich, 2003), resulting in smaller-unit runoff discharge and lower erosion ability.  
382 When the drainage area is larger than 25 km<sup>2</sup>, the unfavorable effects of a wider channel and gentler  
383 gradient on post-fire debris flows might surpass the favorable effect of wildfire, resulting in no  
384 response to the wildfire.

### 385 **5.5 Human activity**

386 In addition to the wildfire set accidentally by people, the construction of the Xiangcheng-Derong  
387 road is another important factor for the amplification of debris flows. The Xiangcheng-Derong road  
388 crosses the port on the eastern border and stretches along the main channel from the outlet of channel  
389 No. 5. Approximately 13.64 km is distributed in the Reneyong watershed, and abundant spoils were  
390 produced when it was constructed. These spoils were deposited on the southern slope of the main  
391 channel with a gradient slightly larger than the friction angle and only a few retaining walls; thus, some  
392 of them have reached the main channel, resulting in a narrowing of the channel. Spoils can also be  
393 found in some other branches. The spoils are composed of fine-grained particles and are only slightly  
394 covered by vegetation because of the arid climate. Although spoils outside the main channel were not  
395 affected by the wildfire, these spoils are still arid, with low hydraulic conductivity owing to long-term  
396 drought (Moody and Ebel, 2012; Sheridan et al, 2016). Low rainfall intensity is required to trigger  
397 surface water runoff and the consequent debris flows (Coe et al., 2008; Kean et al., 2011), which can  
398 partly or wholly block the channel (Fig. 14). This narrowed channel can also be blocked by the large  
399 trunks carried by debris flows.

400 At the narrowed channel section, the debris flows would have a greater depth, resulting in an  
401 increase in the debris flow velocity and greatly enhancing the subsequent erosion ability. A large  
402 amount of the erodible spoils was enrolled by the debris flows, significantly amplifying the magnitude  
403 (Cui et al., 2013; Iverson and Ouyang, 2015). After DF1, abundant spoils were entrained by the debris



404 flows, and remnants of the deposited spoils can be found in a steep section 2~4 m high(Fig. 15). From  
405 the outlet of branch No. 3, there were more than 10 narrowed channel sections; one would induce a  
406 significant entrainment process that could amplify debris flows.

## 407 **6. Conclusion**

408 The existing research on post-wildfire debris flows focuses mainly on the decline in hydraulic  
409 conductivity resulting from the increase in soil water repellency (Doerr and Thomas, 2000; MacDonald  
410 and Huffman, 2004; Doerr et al., 2006; Nyman et al., 2010), the process of soil sealing(Larsen et al.,  
411 2009; Woods and Balfour, 2010), and the low rainfall intensity needed to produce surface water runoff  
412 and trigger debris flows. In addition, the geologic and geomorphic characteristic of the catchment that  
413 may not be affected by wildfire can still produce favorable effects for the magnitude and frequency of  
414 debris flows as follows: 1) The arid climate can reduce the soil water content and hydraulic  
415 conductivity, which can have a positive effect on debris flows, as soil water repellency will quickly  
416 decrease after rainfall; in addition, the arid climate leads to slow vegetation recovery. 2) The deep  
417 weathered remnant of sandy slate has high fine-particle content and high susceptibility to debris flow  
418 entrainment; therefore, the watershed is charged with abundant sediment. 3) The “gentle-steep-gentle”  
419 gradient can contribute to greater surface water runoff and the subsequent severe erosion process in the  
420 steep area. 4) The downward erosion of debris flows in the steep branches generates successive bank  
421 failure, which amplifies debris flows. 5) Statistics show that post-fire debris flows tend to occur in  
422 catchments smaller than 5 km<sup>2</sup> (Cannon et al., 2010) and debris flows in smaller watersheds are apt to  
423 be triggered by a higher rainfall threshold, such as for branches No. 1 and No. 2.

424

## 425 **Acknowledgements**

426 This research was supported by the National Natural Science Foundation of China (grant Nos.  
427 41661134012 and 41402283). We wish to acknowledge the editors of the Natural Hazards and Earth  
428 System Science Editorial Office and the anonymous reviewers for their constructive comments, which  
429 helped us improve the content and presentation of the manuscript.

## 430 **References**

431 Bovis, M. J. and Jakob, M.: The role of debris supply conditions in predicting debris flow activity. Earth



- 432 Surface Processes Landforms 24, 1039-1054, 1999.
- 433 Cannon, S. H. and Gartner, J. E.: Wildfire-related debris flow from a hazards perspective. In Jakob, M.  
434 and Hungr, O., Debris-flow hazards and related phenomena (pp. 363-385). Springer Berlin Heidelberg,  
435 2005.
- 436 Cannon, S. H., Gartner, J. E., Rupert, M. G., Michael, J. A., Rea, A. H., and Parrett, C.: Predicting the  
437 probability and volume of postwildfire debris flows in the intermountain western United  
438 States. Geological Society of America Bulletin, 122, 127-144, 2010.
- 439 Cannon, S. H., Gartner, J. E., Wilson, R. C., Bowers, J. C., and Laber, J. L.: Storm rainfall conditions  
440 for floods and debris flows from recently burned areas in southwestern Colorado and southern  
441 California. Geomorphology 96, 250-269, 2008.
- 442 Cannon, S. H.: Debris-flow generation from recently burned watersheds. Environmental & Engineering  
443 Geoscience 7, 321-341, 2001.
- 444 Cannon, S. H., Kirkham, R. M., and Parise, M.: Wildfire-related debris-flow initiation processes, Storm  
445 King Mountain, Colorado. Geomorphology 39, 171-188, 2001.
- 446 Carretier, S., Regard, V., Vassallo, R., Aguilar, G., Martinod, J., Riquelme, R., ... and Guyot, J. L.:  
447 Slope and climate variability control of erosion in the Andes of central Chile. Geology 41, 195-198,  
448 2013.
- 449 Chen, J. C., Huang, W. S., Jan, C. D., and Yang, Y. H.: Recent changes in the number of rainfall events  
450 related to debris-flow occurrence in the Chenyulan Stream Watershed, Taiwan. Natural Hazards and  
451 Earth System Science 12, 1539-1549, 2012.
- 452 Chow, V. T., Maidment, D. R., and Mays, L. W.: Applied hydrology, McGraw-Hill Inc., Singapore,  
453 1988.
- 454 Cui, P., Zhou, G. G., Zhu, X. H., and Zhang, J. Q.: Scale amplification of natural debris flows caused  
455 by cascading landslide dam failures. Geomorphology 182, 173-189, 2013.
- 456 Coe, J. A., Kinner, D. A., and Godt, J. W.: Initiation conditions for debris flows generated by runoff at  
457 Chalk Cliffs, central Colorado. Geomorphology 96, 270-297, 2008.
- 458 Conedera, M., Peter, L., Marxer, P., Forster, F., Rickenmann, D., and Re, L. Consequences of forest  
459 fires on the hydrogeological response of mountain catchments: a case study of the Riale Buffaga,  
460 Ticino, Switzerland. Earth Surface Processes Landforms 28, 117-129, 2003.
- 461 Dai, F. C., and Lee, C. F. Frequency–volume relation and prediction of rainfall-induced



- 462 landslides. *Engineering geology*, 59, 253-266, 2001.
- 463 DeGRAFF, J. V., Cannon, S. H., Gartner, J. E.: The timing of susceptibility to post-fire debris flows in  
464 the Western United States. *Environmental Engineering Geoscience* 21, 277-292, 2015.
- 465 Doerr, S. H., Shakesby, R. A., Blake, W. H., Chafer, C. J., Humphreys, G. S., and Wallbrink, P. J.:  
466 Effects of differing wildfire severities on soil wettability and implications for hydrological  
467 response. *Journal of Hydrology* 319, 295-311, 2006.
- 468 Doerr, S. H., Shakesby, R. A., and Walsh, R. P. D.: Soil water repellency: its causes, characteristics and  
469 hydro-geomorphological significance. *Earth-Science Review* 51, 33-65, 2000.
- 470 Foster, G. R., and Meyer, L. D. A closed-form soil erosion equation for upland areas. In: Shen, H. W.  
471 (Ed.), *Sedimentation: Symposium to Honor Professor H.A. Einstein*. Colorado State University, Fort  
472 Collins, CO, 1972.
- 473 Gartner, J. E., Cannon, S. H., Santi, P. M., and Dewolfe, V. G.: Empirical models to predict the volumes  
474 of debris flows generated by recently burned basins in the western US. *Geomorphology*, 96(3),  
475 339-354, 2008.
- 476 Gartner, J. E., Cannon, S. H., Biagio, E. R., Davis, N. K., McDonald, C., Pierce, K. L., and Rupert, M.  
477 G.: *Compilation of Basin Morphology, Burn Severity, Soils and Rock Type, Erosive Response,  
478 Debris-flow Initiation Process, and Event-triggering Rainfall for 599 Recently Burned Basins in the  
479 Western U.S. (USGS Open-File Report)*. US Geological Survey, Reston, VA, 2005.
- 480 Guo, X. J., Li, Y., and Cui, P.: Exponential Amplification Effect of Rainfall on Slope Failures in Debris  
481 Flow Source region. *Mountain Research*, 31(4):406-412, 2013. (In Chinese)
- 482 Hungr, O., McDougall, S., Bovis, M.: Entrainment of material by debris flows. In *Debris-flow hazards  
483 and related phenomena*, In *Debris-flow hazards and related phenomena* (pp. 135-158). Springer Berlin  
484 Heidelberg, 2005.
- 485 Iverson, R. M., Reid, M. E., Logan, M., LaHusen, R. G., Godt, J. W., and Griswold, J. P.: Positive  
486 feedback and momentum growth during debris-flow entrainment of wet bed sediment. *Nature  
487 Geoscience* 4, 116-121, 2011.
- 488 Iverson, R. M. and Ouyang, C.: Entrainment of bed material by Earth-surface mass flows: Review and  
489 reformulation of depth-integrated theory. *Review of Geophysics* 53, 27-58, 2015.
- 490 Jakob, M., Bovis, M., and Oden, M. The significance of channel recharge rates for estimating  
491 debris-flow magnitude and frequency. *Earth Surface Processes Landforms* 30, 755-766, 2005.



- 492 Jordan, P.: Post-wildfire debris flows in southern British Columbia, Canada. *International Journal of*  
493 *Wildland Fire* 25, 322-336, 2016.
- 494 Kean, J. W., McCoy, S. W., Tucker, G. E., Staley, D. M., and Coe, J. A.: Runoff-generated debris flows:  
495 Observations and modeling of surge initiation, magnitude, and frequency. *Journal of Geophysical*  
496 *Research-Earth surface* 118, 2190-2207, 2013.
- 497 Kean, J. W., Staley, D. M., and Cannon, S. H.: In situ measurements of post-fire debris flows in  
498 southern California: Comparisons of the timing and magnitude of 24 debris-flow events with rainfall  
499 and soil moisture conditions. *Journal of Geophysical Research-Earth surface* 116(F04019), 2011.
- 500 Lane, P. N., Sheridan, G. J., Noske, P. J.: Changes in sediment loads and discharge from small  
501 mountain catchments following wildfire in south eastern Australia. *Journal of Hydrology* 331, 495-510,  
502 2006.
- 503 Larsen, I. J., MacDonald, L. H., Brown, E., Rough, D., Welsh, M. J., Pietraszek, J. H., ... Schaffrath, K.:  
504 Causes of post-fire runoff and erosion: water repellency, cover, or soil sealing?. *Soil Science Society of*  
505 *America Journal* 73, 1393-1407, 2009.
- 506 MacDonald, L. H., and Huffman, E. L.: Post-fire soil water repellency. *Soil Science Society of America*  
507 *Journal* 68, 1729-1734, 2004.
- 508 McCoy, S. W., Kean, J. W., Coe, J. A., Tucker, G. E., Staley, D. M., and Wasklewicz, T. A.: Sediment  
509 entrainment by debris flows: In situ measurements from the headwaters of a steep catchment. *Journal*  
510 *of Geophysical Research-Earth surface* 117(F03016), 2012.
- 511 Moody, J. A. and Ebel, B. A.: Hyper-dry conditions provide new insights into the cause of extreme  
512 floods after wildfire. *Catena* 93, 58-63, 2012.
- 513 Moody, J. A., Ebel, B. A.: Infiltration and runoff generation processes in fire-affected  
514 soils. *Hydrological Processes* 28, 3432-3453, 2014.
- 515 Moody, J. A., Ebel, B. A., Nyman, P., Martin, D. A., Stoof, C., and McKinley, R.: Relations between  
516 soil hydraulic properties and burn severity. *International Journal of Wildland Fire* 25, 279-293, 2016.
- 517 Moody, J. A., Shakesby, R. A., Robichaud, P. R., Cannon, S. H., and Martin, D. A.: Current research  
518 issues related to post-wildfire runoff and erosion processes. *Earth Science Reviews* 122, 10-37, 2013.
- 519 Ni, H., Zheng, W., Song, Z., and Xu, W.: Catastrophic debris flows triggered by a 4 July 2013 rainfall  
520 in Shimian, SW China: formation mechanism, disaster characteristics and the lessons learned.  
521 *Landslides*, 11(5): 909-921, 2014.



- 522 Noske, P. J., Nyman, P., Lane, P. N., and Sheridan, G. J.: Effects of aridity in controlling the magnitude  
523 of runoff and erosion after wildfire. *Water Resource Research* 52, 4338-4357, 2016.
- 524 Nyman, P., Sheridan, G., and Lane, P. N.: Synergistic effects of water repellency and macropore flow  
525 on the hydraulic conductivity of a burned forest soil, south-east Australia. *Hydrological Processes* 24,  
526 2871-2887, 2016.
- 527 Nyman, P., Smith, H. G., Sherwin, C. B., Langhans, C., Lane, P. N., and Sheridan, G. J.: Predicting  
528 sediment delivery from debris flows after wildfire. *Geomorphology* 250, 173-186, 2015.
- 529 Onda, Y., Dietrich, W. E., and Booker, F.: Evolution of overland flow after a severe forest fire, Point  
530 Reyes, California. *Catena* 72, 13-20, 2008.
- 531 Orem, C. A., and Pelletier, J. D.: The predominance of post-wildfire erosion in the long-term  
532 denudation of the Valles Caldera, New Mexico. *Journal of Geophysical Research-Earth surface* 121,  
533 843-864, 2016.
- 534 Parise, M., and Cannon, S.H.: Wildfire impacts on the processes that generate debris flows in burned  
535 watersheds. *Natural Hazards* 61, 217-227, 2012.
- 536 Robichaud, P. R.: Fire effects on infiltration rates after prescribed fire in Northern Rocky Mountain  
537 forests, USA. *Journal of Hydrology* 231, 220-229, 2000.
- 538 Santi, P. M., Higgins, J. D., Cannon, S.H., and Gartner, J. E. Sources of debris flow material in burned  
539 areas. *Geomorphology* 96, 310-321, 2008.
- 540 Sheridan, G. J., Nyman, P., Langhans, C., Cawson, J., Noske, P. J., Oono, A., ... Lane, P.N.: Is aridity a  
541 high-order control on the hydro-geomorphic response of burned landscapes?. *International Journal of*  
542 *Wildland Fire* 25, 262-267, 2016.
- 543 Smith, H. G., Sheridan, G. J., Lane, P. N., and Sherwin, C. B.: Paired Eucalyptus forest catchment  
544 study of prescribed fire effects on suspended sediment and nutrient exports in south-eastern  
545 Australia. *International Journal of Wildland Fire* 19, 624-636, 2010.
- 546 Staley, D. M., Kean, J. W., Cannon, S. H., Schmidt, K. M., and Laber, J. L.: Objective definition of  
547 rainfall intensity-duration thresholds for the initiation of post-fire debris flows in southern  
548 California. *Landslides* 10, 547-562, 2013.
- 549 Staley, D. M., Wasklewicz, T. A., Kean, J. W.: Characterizing the primary material sources and  
550 dominant erosional processes for post-fire debris-flow initiation in a headwater basin using  
551 multi-temporal terrestrial laser scanning data. *Geomorphology* 214, 324-338, 2014.



- 552 Stock, J., and Dietrich, W. E.: Valley incision by debris flows: Evidence of a topographic  
553 signature. *Water Resource Research*, 39, 1089, 2003.
- 554 Stoof, C. R., Vervoort, R. W., Iwema, J., Van, E., Ferreira, A. J. D., and Ritsema, C. J.: Hydrological  
555 response of a small catchment burned by experimental fire. *Hydrology and Earth System Sciences* 16,  
556 267-285, 2012.
- 557 Tan, W. P., Wang, C. H., and Jing Y. T.: Regional prediction and forecast of storm induced debris flows  
558 and landslide. Sichuan Press of Science and Technology, Chengdu, 1994.
- 559 Tang, C., Yang, Y., Su, Y., Ding, J., and Huang, W.: The disastrous 23 July 2009 debris flow in  
560 Xiangshui gully, Kangding county, Southwestern China[J]. *Journal of Mountain Science*, 8: 131-139,  
561 2011.
- 562 Wondzell, S. M., and King, J. G. Postfire erosional processes in the Pacific Northwest and Rocky  
563 Mountain regions. *Forest Ecology Management* 178, 75-87, 2003.
- 564 Woods, S. W., and Balfour, V. N. The effects of soil texture and ash thickness on the post-fire  
565 hydrological response from ash-covered soils. *Journal of Hydrology* 393, 274-286, 2010.
- 566 VanDine, D. F., Rodman, R. F., Jordan, P., and Dupas, J.: Kuskonook Creek, an example of a debris  
567 flow analysis. *Landslides* 2, 257-265, 2005.
- 568 Ziemer, R. R.: Roots and the stability of forested slopes: International Association of Hydrologic  
569 Science 132, 343-357, 1981.
- 570 Zhu, X. H.: Study on erosion characteristics and routing of debris flow along the channel. Graduate  
571 University of Chinese Academy of Sciences. Doctor thesis, 2013. (In Chinese)
- 572 Zhang, J. Q., Cui, P., Ge, Y. G., and Hong, Y.: Relationship between rainfall characteristics and total  
573 amount of debris flow. *Journal of Beijing Forestry University*, 31, 77-83, 2009. (In Chinese)
- 574



575

Table 1. Geographic information for branches No.1~No.3

No.	Drainage area (km <sup>2</sup> )	Maximum basin relief (m)	Gradient (degrees)	Gradient (central part) (degrees)	Gradient (upper part) (degrees)
Branch No.1	0.37	544	27	32	18
Branch No.2	0.73	755	26	35	18
Branch No.3	2.30	836	15	20	14

576



577

Table 2. Basic information regarding the debris flows

No.	Time	Location	Recorded 3-day antecedent precipitation(mm)	Debris flow volume (1000 m <sup>3</sup> )
DF1	16:08, June 8, 2014	No. 3	1.11	86.2
DF2	16:00, June 30, 2014	No. 3	14.84	5.1
DF3	23:20, July 10, 2014	No. 3	0.81	32.3
DF4	19:43, August 24, 2015	No.1, No.2 and No.3	39.97	154.5

578



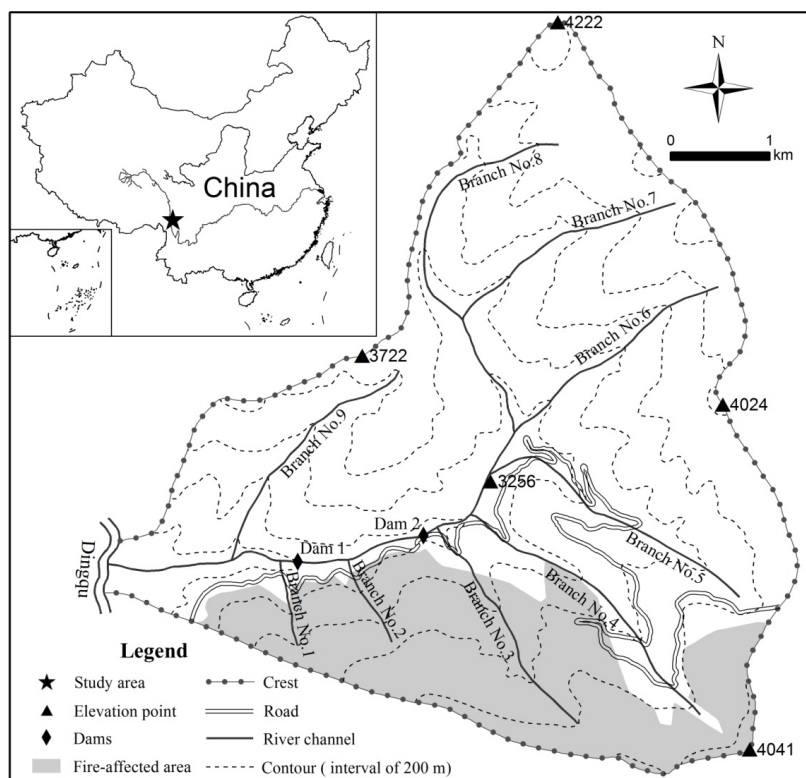
579

Table 3. Basic information regarding the three rain gauges

No.	Name	Location	Elevation (m)	Distance (km)	Precision (mm)	$\omega_i$
1	Zhengdou	29°08'N, 99°33'E	2858	3.90	0.1	0.60
2	Reda	29°06'N, 99°38'E	3363	5.56	0.1	0.30
3	Adu	29°11'N, 99°39'E	2783	9.40	0.1	0.10

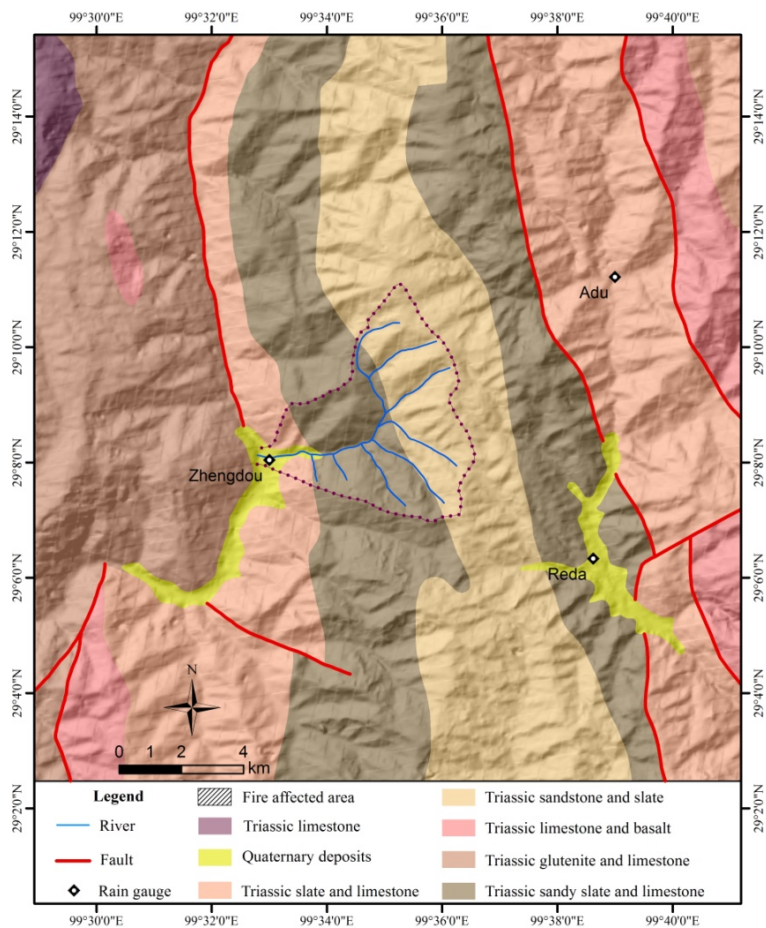
580

581



582  
583

Figure. 1. Location of Reneyong Valley and related geographic features



584

585

Figure 2. Simplified geologic map and distribution of applied rainfall gauges



586

587

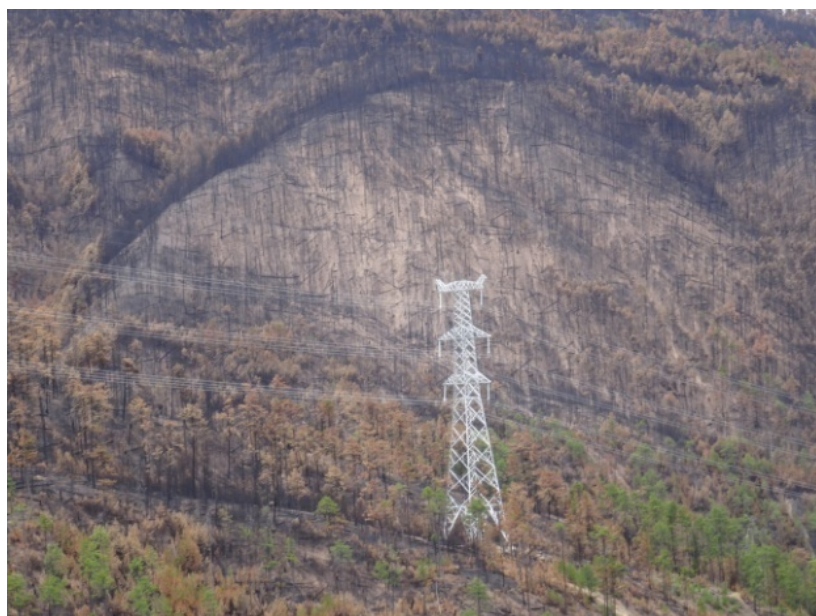
Figure 3. Houses destroyed by debris flows in the downstream



588

589

Figure 4. Road buried by debris flows from branch No. 3



590

591

Figure 5. Overlooking the fire-affected area



592

593

594

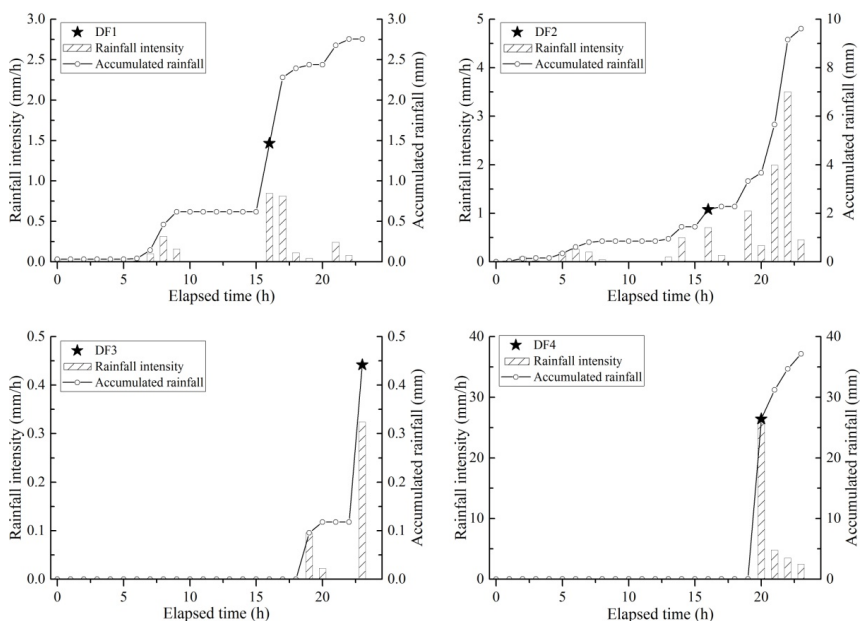
Figure 6. Trough test in the fire-affected area



595

596

Figure 7. Particle size measurement of debris flow deposits (DF1)



597

598 Figure 8. Recorded rainfall prior to the debris flows(rainfall data from theZhengdou, Reda and Adu rain

599

gauges were applied)

600



601

602

Figure 9. Upstream of branch No. 3 after DF1 (no debris flow remnants)



603

604

Figure 10. Middle stream of branch No. 3 after DF1



605

606

Figure 11. Branch No. 2 after DF4



607  
608  
609

Figure 12. Branch No. 1 after DF4



610

611 Figure 13. Debris flow deposits of (a) DF1 in the Dingqu River, (b) DF2 slightly striking the borehole

612 instrument, (c) DF3 partly blocking the Dingqu River, and d) DF4 intercepted by check dam 2



613

614

Figure 14. The main channel narrowed by spoil and spoil-induced debris flows



615

616

Figure 15. Remnants of a spoil dam after debris flows